

Dynamic properties of the spin- $\frac{1}{2}$ XY chain with three-site interactions

Taras Krokhmalkii,^{1,2} Oleg Derzhko,^{1,2} Joachim Stolze,² and Taras Verkholyak^{1,2}

¹*Institute for Condensed Matter Physics, National Academy of Sciences of Ukraine, 1 Svientsitskii Street, L'viv-11 79011, Ukraine*

²*Institut für Physik, Technische Universität Dortmund, 44221 Dortmund, Germany*

(Received 15 February 2008; published 2 May 2008)

We consider a spin- $\frac{1}{2}$ XY chain in a transverse (z) field with multisite interactions. The additional terms introduced into the Hamiltonian involve products of spin components related to three adjacent sites. A Jordan–Wigner transformation leads to a simple bilinear Fermi form for the resulting Hamiltonian and, hence, the spin model admits a rigorous analysis. We point out the close relationships between several variants of the model, which were discussed separately in previous studies. The ground-state phases (ferromagnet and two kinds of spin liquid) of the model are reflected in the dynamic structure factors of the spin chains, which are the main focus in this study. First, we consider the zz dynamic structure factor, reporting for this quantity a closed-form expression and analyzing the properties of the two-fermion (particle-hole) excitation continuum, which governs the dynamics of transverse spin component fluctuations and of some other local operator fluctuations. Then we examine the xx dynamic structure factor, which is governed by many-fermion excitations, reporting both analytical and numerical results. We discuss some easily recognized features of the dynamic structure factors, which are signatures of the presence of the three-site interactions.

DOI: [10.1103/PhysRevB.77.174404](https://doi.org/10.1103/PhysRevB.77.174404)

PACS number(s): 75.10.Jm, 75.40.Gb

I. MULTISITE INTERACTIONS AND JORDAN–WIGNER FERMIONIZATION

Spin- $\frac{1}{2}$ XY chains provide an excellent ground for studying various properties of quantum many-particle systems since, after performing the Jordan–Wigner transformation, these spin models can be reduced to systems of noninteracting spinless fermions.¹ One interesting issue that has recently emerged in the theory of quantum spin systems is the study of effects of multisite interspin interactions. Such interactions may arise, e.g., in an effective spin model for the standard Hubbard model at half filling in higher orders (beyond t^2/U) of the strong-coupling t/U expansion.² Another example is provided by quantum spin systems with energy currents.^{3–5} As early as 1971,⁶ Suzuki proposed generalized one-dimensional XY models with multisite interactions, which allows for a rigorous analysis by the Jordan–Wigner fermionization approach. An exactly integrable spin- $\frac{1}{2}$ XXZ quantum spin chain with three-site interactions was suggested in Ref. 7 (see also Ref. 8). An XY version of this model was independently considered in Ref. 9. Another version of the spin- $\frac{1}{2}$ XY chain with three-site interactions was suggested in Refs. 10 and 11. Later on, spin- $\frac{1}{2}$ XY chains with three-site interactions were considered in a number of papers concerning quantum phase transitions, transport properties, and entanglement.^{12–20} Recently, in Ref. 21, the spin- $\frac{1}{2}$ XY chain with alternating three-site interaction has been introduced, whereas in Ref. 22, the dynamic characteristics of a few quantum spin chains with multisite interactions have been discussed. However, an exhaustive study of the dynamic properties of spin- $\frac{1}{2}$ XY chains with multisite interactions, similar to that for conventional XY chains,^{23–25} has not been performed yet. With our paper, we attempt to fill this gap.

In what follows, we consider the Hamiltonian

$$H = \sum_n [J_n (s_n^x s_{n+1}^x + s_n^y s_{n+1}^y) + D_n (s_n^x s_{n+1}^y - s_n^y s_{n+1}^x)] + K_n (s_n^x s_{n+1}^z s_{n+2}^x + s_n^y s_{n+1}^z s_{n+2}^y) + E_n (s_n^x s_{n+1}^z s_{n+2}^y - s_n^y s_{n+1}^z s_{n+2}^x) + \Omega_n s_n^z. \quad (1.1)$$

Here, J_n and D_n are the isotropic XY (or XX) exchange interaction and the z component of the Dzyaloshinskii–Moriya interaction between the neighboring sites n and $n+1$, respectively. K_n and E_n are two types of three-site exchange interactions introduced in Refs. 10 and 11 and in Ref. 9, respectively [see also Ref. 26 where the general Hamiltonian (1.1) was introduced as well]. Ω_n is the transverse (z) external magnetic field at site n . The sum in Eq. (1.1) runs over all N lattice sites; boundary conditions (open or periodic) are not important for the quantities to be calculated in the thermodynamic limit $N \rightarrow \infty$. In this study, in most cases, we restrict ourselves to homogeneous chains with site-independent values of the interspin interaction constants and field, i.e., $J_n = J$.

We start by discussing the symmetry properties of the Hamiltonian (1.1) in order to show the close relations between the models of Ref. 9 (i.e., with the XZY–YZX type of three-site interactions) and of Refs. 10 and 11 (i.e., with the XZX+YZY type of three-site interactions), which were not discussed before. Consider a local spin rotation around the z axis

$$s_n^x \rightarrow \tilde{s}_n^x = s_n^x \cos \phi_n + s_n^y \sin \phi_n, \\ s_n^y \rightarrow \tilde{s}_n^y = -s_n^x \sin \phi_n + s_n^y \cos \phi_n, \\ s_n^z \rightarrow \tilde{s}_n^z = s_n^z. \quad (1.2)$$

Under that transformation, the parameters for the interspin interactions in the Hamiltonian (1.1) are mapped as follows:

$$J_n \rightarrow \tilde{J}_n = J_n \cos(\phi_{n+1} - \phi_n) + D_n \sin(\phi_{n+1} - \phi_n),$$

$$\begin{aligned}
D_n &\rightarrow \tilde{D}_n = -J_n \sin(\phi_{n+1} - \phi_n) + D_n \cos(\phi_{n+1} - \phi_n), \\
K_n &\rightarrow \tilde{K}_n = K_n \cos(\phi_{n+2} - \phi_n) + E_n \sin(\phi_{n+2} - \phi_n), \\
E_n &\rightarrow \tilde{E}_n = -K_n \sin(\phi_{n+2} - \phi_n) + E_n \cos(\phi_{n+2} - \phi_n).
\end{aligned} \tag{1.3}$$

This shows clearly that the rotations (1.2) may be employed to simplify the Hamiltonian (1.1) by eliminating some of the interactions. For example, in a homogeneous chain, we may achieve $\tilde{D}=0$ by setting $\phi_{n+1}-\phi_n=\varphi$ with $\tan \varphi = D/J$.²⁷ The remaining coupling constants then are $\tilde{J} = \text{sgn}(J)\sqrt{J^2+D^2}$, $\tilde{K} = [(J^2-D^2)K+2JDE]/(J^2+D^2)$, and $\tilde{E} = [-2JDK+(J^2-D^2)E]/(J^2+D^2)$.

More interestingly, by using Eqs. (1.2) and (1.3), we can eliminate from the Hamiltonian Eq. (1.1) either of the three-site interactions, K_n or E_n . By introducing $\theta_n = \phi_{n+2} - \phi_n$, we note that $\tilde{K}_n=0$ if $\tan \theta_n = -K_n/E_n$. These θ_n values can be used to calculate the \tilde{J}_n and \tilde{D}_n by using $\phi_{2m} - \phi_{2m-1} = \phi_2 - \phi_1 + \sum_{j=1}^{m-1} (\theta_{2j} - \theta_{2j-1})$ and $\phi_{2m+1} - \phi_{2m} = \theta_{2m-1} - \phi_{2m} + \phi_{2m-1}$; the surviving three-site coupling is $\tilde{E}_n = \text{sgn}(E_n)\sqrt{E_n^2 + K_n^2}$. If, on the other hand, we set $\tan \theta_n = E_n/K_n$, we get $\tilde{E}_n=0$, whereas $\tilde{K}_n = \text{sgn}(K_n)\sqrt{K_n^2 + E_n^2}$. For the uniform chain, on which we mainly focus in what follows, $\theta_n = \theta$, $\phi_{2m} - \phi_{2m-1} = \phi_2 - \phi_1$, and $\phi_{2m+1} - \phi_{2m} = \theta - \phi_2 + \phi_1$, and assuming $\phi_2 - \phi_1 = \theta/2$, we get $\tilde{J} = J \cos(\theta/2) + D \sin(\theta/2)$, $\tilde{D} = -J \sin(\theta/2) + D \cos(\theta/2)$, and either $\tilde{K}=0$, $\tilde{E} = \text{sgn}(E)\sqrt{K^2 + E^2}$ if $\tan \theta = -K/E$ or $\tilde{E}=0$, $\tilde{K} = \text{sgn}(K)\sqrt{K^2 + E^2}$ if $\tan \theta = E/K$.

To summarize this part, we have shown that while studying the effects of three-site interactions on the basis of the model (1.1), it would be sufficient to consider the model (1.1) with either nonzero parameters J_n, D_n, K_n or J_n, D_n, E_n since the most general case when all four types of interactions have nonzero values can be reduced either to the former case or to the latter case. One consequence of this is that the model considered in Ref. 11 can be reduced to the model considered in Ref. 9. Namely, starting from the model with $J \neq 0, K \neq 0$, and $D=E=0$, and choosing $\phi_{n+2}-\phi_n=\pi/2$, $\phi_{n+1}-\phi_n=\pi/4$, and $\phi_n=n\pi/4$, we arrive at the model with $\tilde{J}=J/\sqrt{2}$, $\tilde{D}=-J/\sqrt{2}$, $\tilde{E}=-K$, and $\tilde{K}=0$. Vice versa, starting from the model with $J \neq 0, D \neq 0, E \neq 0$, and $K=0$, and performing the same transformation, we arrive at the model with $\tilde{J}=(J+D)/\sqrt{2}$, $\tilde{D}=(-J+D)/\sqrt{2}$, $\tilde{K}=E$, and $\tilde{E}=0$. In our study of the dynamic properties of quantum spin chains with three-site interactions, we focus on the case $J \neq 0, K \neq 0$, and $D=E=0$, leaving a detailed study of other cases for the future.

The peculiar nature of the three-site interactions studied here becomes clear after performing the Jordan–Wigner transformation

$$\begin{aligned}
s_n^+ &= s_n^x + i s_n^y = P_{n-1} c_n^\dagger, & s_n^- &= s_n^x - i s_n^y = P_{n-1} c_n, \\
c_n^\dagger &= P_{n-1} s_n^+, & c_n &= P_{n-1} s_n^-,
\end{aligned}$$

$$P_m = \prod_{j=1}^m (1 - 2c_j^\dagger c_j) = \prod_{j=1}^m (-2s_j^z). \tag{1.4}$$

By substituting Eq. (1.4) into Eq. (1.1), we find

$$\begin{aligned}
H = \sum_n &\left[\frac{J_n + iD_n}{2} c_n^\dagger c_{n+1} + \frac{J_n - iD_n}{2} c_{n+1}^\dagger c_n - \frac{K_n + iE_n}{4} c_n^\dagger c_{n+2} \right. \\
&\left. - \frac{K_n - iE_n}{4} c_{n+2}^\dagger c_n + \Omega_n \left(c_n^\dagger c_n - \frac{1}{2} \right) \right],
\end{aligned} \tag{1.5}$$

i.e., the Hamiltonian of the spin model is a simple bilinear form in terms of spinless fermions. For the uniform case, it is convenient to employ periodic boundary conditions in the spin Hamiltonian (1.1), which leads either to periodic or antiperiodic boundary conditions in the fermion Hamiltonian (1.5), depending on whether the number of spinless fermions is even or odd. Either the nearest-neighbor hopping integrals or the next-nearest-neighbor hopping integrals can be made real (or purely imaginary) by applying a gauge transformation, which is the analog of Eqs. (1.2) and (1.3) in the spinless-fermion picture.

In the uniform case, we can diagonalize Eq. (1.5) by performing the Fourier transformation

$$c_n^\dagger = \frac{1}{\sqrt{N}} \sum_{\kappa} \exp(i\kappa n) c_\kappa^\dagger, \quad c_n = \frac{1}{\sqrt{N}} \sum_{\kappa} \exp(-i\kappa n) c_\kappa, \tag{1.6}$$

with $\kappa = (2\pi/N)m$ [$\kappa = (2\pi/N)(m+1/2)$] in the subspaces with odd [even] numbers of spinless fermions and $m = -N/2, -N/2+1, \dots, N/2-1$ (if N is even) or $m = -(N-1)/2, -(N-1)/2+1, \dots, (N-1)/2$ (if N is odd) arriving at

$$\begin{aligned}
H &= \sum_{\kappa} \Lambda_{\kappa} \left(c_{\kappa}^\dagger c_{\kappa} - \frac{1}{2} \right), \\
\Lambda_{\kappa} &= J \cos \kappa + D \sin \kappa - \frac{K}{2} \cos(2\kappa) - \frac{E}{2} \sin(2\kappa) + \Omega.
\end{aligned} \tag{1.7}$$

From Eq. (1.7), we immediately conclude that the external magnetic field Ω plays the role of a chemical potential for spinless fermions. More interestingly, the two terms proportional to $\cos(2\kappa)$ and $\sin(2\kappa)$ in the elementary excitation spectrum Λ_{κ} (1.7), which arise from the three-site spin interactions, may drastically modify Λ_{κ} , leading to additional ground-state [GS] phases. We consider the case $J \neq 0, K \neq 0$, and $D=E=0$; for this case, $\Lambda_{-\kappa} = \Lambda_{\kappa}$. As long as $|K| < |J|/2$, the spinless-fermion system may possess only two Fermi points, whereas for sufficiently strong three-site interaction, $|K| > |J|/2$, the spinless fermion system may also possess four Fermi points. The ground-state phase diagram obtained in Ref. 11 is shown in Fig. 1. Two different spin liquid phases reflect the importance of the existence of two versus four Fermi points, as discussed already earlier.¹¹ As a result, in addition to the conventional quantum phase transition between the spin liquid I phase and the ferromagnetic phase, the spin model may exhibit also quantum phase tran-

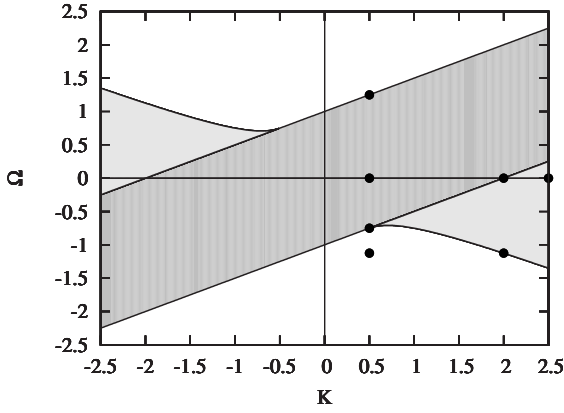


FIG. 1. The ground-state phase diagram of the homogeneous model (1.1) with $J = \pm 1$, $K \neq 0$, and $D = E = 0$ discussed earlier in Ref. 11. The region $-1 + K/2 < \Omega < 1 + K/2$ corresponds to the spin liquid I phase [two Fermi points (dark gray)], the regions $K < -1/2$, $1 + K/2 < \Omega < -K/2 - 1/(4K)$ and $K > 1/2$, $-K/2 - 1/(4K) < \Omega < -1 + K/2$ correspond to the spin liquid II phase [four Fermi points (light gray)], and the remaining regions correspond to the ferromagnetic phase (light). The black dots correspond to the sets of parameters that we most often use below to discuss dynamic quantities.

sitions (1) between the spin liquid I phase and the spin liquid II phase and (2) between the spin liquid II phase and the ferromagnetic phase, as well as a point where three phases meet (see Fig. 1). The spin liquid I phase and the spin liquid II phase are characterized by a change in the power-law decay and oscillating factor of spin-spin correlations [see Eqs. (20)–(23) in Ref. 11].

To describe a zero-field quantum phase transition from the spin liquid I to the spin liquid II phase at $|K| = 2|J|$, Titvinidze and Japaridze¹¹ introduced the order parameter η constructed from the average length \bar{L} of the ferromagnetic string in the ground state [see Eqs. (31)–(33) in Ref. 11]. On the other hand, in their study of the (homogeneous) model (1.1) with $J \neq 0$, $E \neq 0$, and $D = K = 0$, Lou *et al.*¹² introduced the scalar chirality parameter $O = -(1/N) \sum_n \langle s_{n-1}^x s_n^y s_{n+1}^z - s_{n-1}^y s_n^z s_{n+1}^x \rangle$ and calculated this quantity in the ground state at $\Omega = 0$ [see Eqs. (10) and (11) in Ref. 12]. A nonzero value of O signals the appearance of a different (chiral) spin liquid phase, which emerges when three-site interactions exceed a critical value. By eliminating $XYZ - YZX$ terms from the Hamiltonian by the unitary transformation discussed above, one arrives at the spin model with $\tilde{J} = J/\sqrt{2}$, $\tilde{D} = -J/\sqrt{2}$, $\tilde{K} = E$, $\tilde{E} = 0$ (i.e., the model similar to the one considered in Ref. 11), and $O \rightarrow \tilde{O} = -(1/N) \sum_n \langle s_{n-1}^x s_n^z s_{n+1}^y + s_{n-1}^y s_n^z s_{n+1}^x \rangle$. The latter quantity \tilde{O} apparently has no relation to the order parameter η used in Ref. 11.

It is also worth mentioning here that the spin model (1.1) can be written as a one-dimensional model of hard-core bosons after introducing the on-site creation and annihilation operators $s_n^+ = s_n^x + i s_n^y$ and $s_n^- = s_n^x - i s_n^y$, $s_n^z = s_n^+ s_n^- - 1/2$. The hard-core boson model is obtained by taking the $U \rightarrow \infty$ limit of the boson Hubbard model. With this mapping, in the case of a conventional transverse XX chain, the ferromagnetic phase corresponds to the Mott insulator with $(1/N) \sum_n \langle s_n^+ s_n^- \rangle$

$= 0$ or $(1/N) \sum_n \langle s_n^+ s_n^- \rangle = 1$ (the thermodynamic average taken at zero temperature, $T = 0$), whereas the spin liquid (spin liquid I) phase is the superfluid with $0 < (1/N) \sum_n \langle s_n^+ s_n^- \rangle < 1$. As a function of the field or chemical potential Ω , the model displays two superfluid to Mott insulator transitions at $\Omega = \pm |J|$.²⁸ After switching on the three-site interaction $K \neq 0$, the picture remains qualitatively the same as long as $|K/J| < 1/2$. If $|K/J|$ exceeds $1/2$, we face an additional transition, which manifests itself as an extra cusp in the dependence of $(1/N) \sum_n \langle s_n^+ s_n^- \rangle$ on Ω . Thus, following the ground-state average boson number per site [or $m_z = (1/N) \sum_n \langle s_n^z \rangle = (1/N) \sum_n \langle s_n^+ s_n^- \rangle - 1/2$] as a function of Ω , one may reproduce the various phases and the phase transitions between them, as shown in Fig. 1. An alternative way to follow the changes in the ground-state dependence of m_z on Ω is to examine the ground-state susceptibility $\chi_{zz} = \partial m_z / \partial \Omega$ as a function of Ω . We notice that the ground-state dependence of $-\chi_{zz}$ on Ω is the same as that of $\rho(E = 0)$ on Ω , where $\rho(E) = (1/N) \sum_\kappa \delta(E - \Lambda_\kappa)$ and $\Lambda_\kappa = J \cos \kappa - (K/2) \cos(2\kappa) + \Omega$ is the one-particle density of states. As a result, the ground-state dependence χ_{zz} vs Ω exhibits a square-root van Hove singularity along the lines separating different phases in Fig. 1. (The only exception are the two points $K = \pm |J|/2$ and $\Omega = \mp |J| + K/2$, at which $\Lambda_\kappa \propto \kappa^4$ and, therefore, χ_{zz} displays a van Hove singularity with the exponent $3/4$.) The divergence of the uniform static zz susceptibility implies a “ferromagnetic” character of the associated phase transitions.

To summarize, there is no doubt that while “the two Fermi point spinless fermions” transform into “the four Fermi point spinless fermions,” some noticeable changes in the properties of the spin model should take place; however, a transparent quantity associated with this modification of the Fermi surface topology, which may play the role of the order parameter, is still lacking.

Finally, it is worth noting the studies on the one-dimensional Hubbard model with next-nearest-neighbor hopping because the noninteracting limit of that model resembles Eq. (1.7) (see, e.g., Ref. 29 and references therein). In contrast to those studies, we calculate two- and many-particle correlation functions [although for a system of noninteracting spinless fermions (1.7)], which are related to two-spin correlation functions for an interacting quantum spin system.

In our study of the dynamic properties of the spin model, we focus on the dynamic structure factor

$$S_{AB}(\kappa, \omega) = \sum_{l=1}^N \exp(-i\kappa l) \int_{-\infty}^{\infty} dt \exp(i\omega t) \langle (A_n(t) - \langle A \rangle) \times (B_{n+l}(0) - \langle B \rangle) \rangle, \quad (1.8)$$

where A_n and B_n are some local operators attached to the site n (like s_n^α , $\alpha = x, y, z$ or $d_n^{(1)} = s_n^x s_{n+1}^x + s_n^y s_{n+1}^y$), $A_n(t) = \exp(iHt) A_n \exp(-iHt)$, $\langle (\dots) \rangle = \text{Tr}[\exp(-\beta H) (\dots)] / \text{Tr} \exp(-\beta H)$, and $\langle A \rangle = (1/N) \sum_n \langle A_n \rangle$. By knowing the dynamic structure factors, we can find the corresponding dynamic susceptibilities according to well known relations (see, e.g., Ref. 30).

In Sec. II, we report a closed-form expression for the zz dynamic structure factor $S_{zz}(\kappa, \omega)$ [i.e., $A_n=B_n=s_n^z$ in Eq. (1.8)] and for some similar dynamic structure factors $S_j(\kappa, \omega)$ [see Eqs. (2.3) and (2.4) below], all of which are governed by two-fermion (particle-hole) excitations. Then, in Sec. III, we discuss the general properties of the two-fermion excitation continuum, focusing on spectral boundaries, soft modes, singularities, etc. We also contrast generic and specific features of various two-fermion dynamic quantities. In Sec. IV, we examine many-fermion dynamic quantities focusing, in particular, on the xx dynamic structure factor $S_{xx}(\kappa, \omega)$ [i.e., $A_n=B_n=s_n^x$ in Eq. (1.8)]. We report exact analytical results (1) in the high-temperature regime $\beta=0$ ($T \rightarrow \infty$) and (2) in the strong-field regime in the ground state as well as precise numerical results for arbitrary temperatures. Finally, in Sec. V, we summarize our findings. Some selected results of the present study were announced in Ref. 31.

II. zz DYNAMIC STRUCTURE FACTOR AND SOME OTHER TWO-FERMION DYNAMIC STRUCTURE FACTORS

We start with the calculation of the transverse dynamic structure factor $S_{zz}(\kappa, \omega)$ that corresponds to $A_n=B_n=s_n^z$ in Eq. (1.8). Since $s_n^z=c_n^\dagger c_n - 1/2$ according to Eq. (1.4), the calculation of the transverse dynamic structure factor is very simple.^{23,32} By using Eqs. (1.6) and (1.7) and the Wick–Bloch–de Dominicis theorem, we end up with the result

$$S_{zz}(\kappa, \omega) = \int_{-\pi}^{\pi} d\kappa_1 n_{\kappa_1} (1 - n_{\kappa_1+\kappa}) \delta(\omega + \Lambda_{\kappa_1} - \Lambda_{\kappa_1+\kappa})$$

$$= \sum_{\kappa_1^*} \left. \frac{n_{\kappa_1} (1 - n_{\kappa_1+\kappa})}{\left| \frac{\partial}{\partial \kappa_1} (\Lambda_{\kappa_1} - \Lambda_{\kappa_1+\kappa}) \right|} \right|_{\kappa_1=\kappa_1^*}. \quad (2.1)$$

Here, $n_\kappa = 1/[1 + \exp(\beta\Lambda_\kappa)]$ is the Fermi function and $\{\kappa_1^*\}$ are the solutions of the equation

$$\omega + \Lambda_{\kappa_1^*} - \Lambda_{\kappa_1^*+\kappa} = 0. \quad (2.2)$$

There are more local spin operators which, in fermionic representation, are given by a product of two Fermi operators,

$$d_n^{(1)} = s_n^x s_{n+1}^x + s_n^y s_{n+1}^y = \frac{1}{2} (c_n^\dagger c_{n+1} - c_n c_{n+1}^\dagger),$$

$$d_n^{(2)} = s_n^x s_{n+1}^y - s_n^y s_{n+1}^x = \frac{i}{2} (c_n^\dagger c_{n+1} + c_n c_{n+1}^\dagger),$$

$$t_n^{(1)} = s_n^x s_{n+1}^z + s_n^y s_{n+1}^z = -\frac{1}{4} (c_n^\dagger c_{n+2} - c_n c_{n+2}^\dagger),$$

$$t_n^{(2)} = s_n^x s_{n+1}^z - s_n^y s_{n+1}^z = -\frac{i}{4} (c_n^\dagger c_{n+2} + c_n c_{n+2}^\dagger), \quad (2.3)$$

and so on. The correlation functions $\langle d_n^{(1)}(t) d_{n+i}^{(1)}(0) \rangle$, $\langle d_n^{(2)}(t) d_{n+i}^{(2)}(0) \rangle$, $\langle t_n^{(1)}(t) t_{n+i}^{(1)}(0) \rangle$, and $\langle t_n^{(2)}(t) t_{n+i}^{(2)}(0) \rangle$ and the cor-

responding structure factors $S_j(\kappa, \omega)$, $S_D(\kappa, \omega)$, $S_K(\kappa, \omega)$, and $S_E(\kappa, \omega)$ therefore can again be easily calculated with the result

$$S_j(\kappa, \omega) = \int_{-\pi}^{\pi} d\kappa_1 B_j(\kappa_1, \kappa_1 + \kappa) C(\kappa_1, \kappa_1 + \kappa)$$

$$\times \delta[\omega - E(\kappa_1, \kappa_1 + \kappa)]$$

$$= \sum_{\kappa_1^*} \left. \frac{B_j(\kappa_1, \kappa_1 + \kappa) C(\kappa_1, \kappa_1 + \kappa)}{\left| \frac{\partial}{\partial \kappa_1} E(\kappa_1, \kappa_1 + \kappa) \right|} \right|_{\kappa_1=\kappa_1^*},$$

$$B_j(\kappa_1, \kappa_2) = \cos^2 \frac{\kappa_1 + \kappa_2}{2},$$

$$B_D(\kappa_1, \kappa_2) = \sin^2 \frac{\kappa_1 + \kappa_2}{2},$$

$$B_K(\kappa_1, \kappa_2) = \frac{1}{4} \cos^2(\kappa_1 + \kappa_2),$$

$$B_E(\kappa_1, \kappa_2) = \frac{1}{4} \sin^2(\kappa_1 + \kappa_2),$$

$$C(\kappa_1, \kappa_2) = n_{\kappa_1} (1 - n_{\kappa_2}),$$

$$E(\kappa_1, \kappa_2) = -\Lambda_{\kappa_1} + \Lambda_{\kappa_2}. \quad (2.4)$$

We note that $S_{zz}(\kappa, \omega)$ (2.1) is also given by Eq. (2.4) with $B_{zz}(\kappa_1, \kappa_2) = 1$.

In Figs. 2–4, we show the grayscale plots for the different two-fermion dynamic structure factors (2.1) and (2.4) for several representative sets of the Hamiltonian parameters, at zero and infinite temperatures. By comparing the closed-form expressions (2.1) and (2.4) and the grayscale plots in Figs. 2–4, we conclude that (1) the generic properties of all these two-fermion dynamic quantities are controlled by the δ function containing $E(\kappa_1, \kappa_2)$ in Eqs. (2.1) and (2.4) in the high-temperature limit $T \rightarrow \infty$ ($\beta \rightarrow 0$), whereas in the low-temperature limit $T \rightarrow 0$ ($\beta \rightarrow \infty$), the factor containing Fermi functions, $C(\kappa_1, \kappa_2)$, becomes important in addition and (2) the specific properties of the various two-fermion dynamic quantities arise only due to different functions $B_j(\kappa_1, \kappa_2)$. In Sec. III, we further examine the two-fermion dynamic structure factors, which reveal their similarities and differences.

III. TWO-FERMION EXCITATION CONTINUUM: GENERIC VERSUS SPECIFIC PROPERTIES

Let us discuss the properties of the two-fermion excitation continuum, which is probed by a number of dynamic quantities such as the transverse dynamic structure factor $S_{zz}(\kappa, \omega)$, the dimer dynamic structure factor $S_j(\kappa, \omega)$, etc. For the model under consideration here, Eq. (1.1) with coupling constants $D=E=0$, the elementary excitation spectrum (1.7) differs from that of the standard homogeneous XX

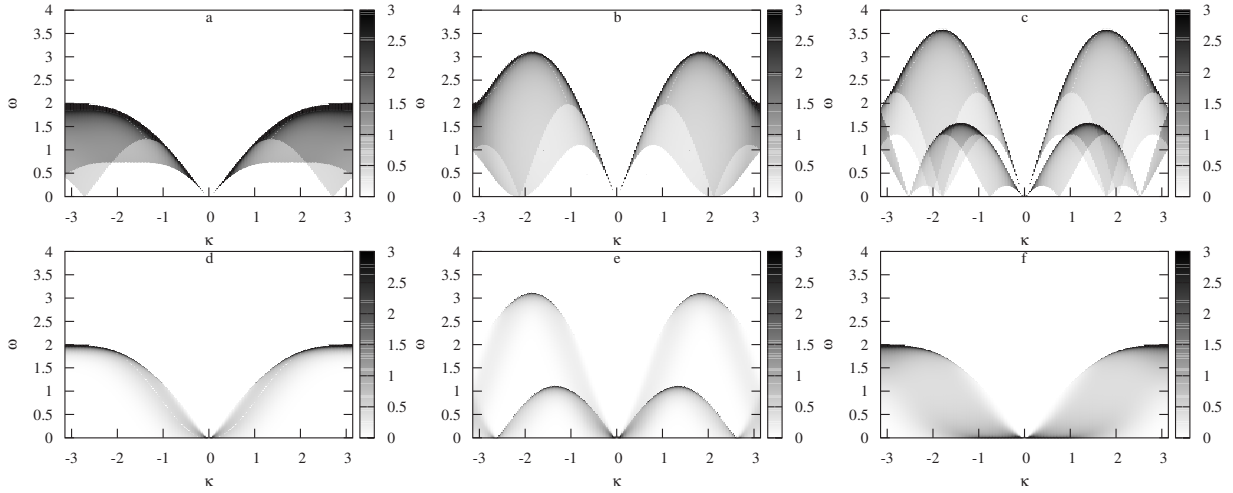


FIG. 2. $S_{zz}(\kappa, \omega)$ for the model (1.1) with $J=1$ and $D=E=0$: (a) $K=0.5$, $\Omega=0$; (b) $K=2$, $\Omega=0$; (c) $K=2.5$, $\Omega=0$; (d) $K=0.5$, $\Omega=1.25$; (e) $K=2$, $\Omega=-1.125$; and (f) $K=0.5$, $\Omega=-0.75$. (a)–(c) refer to the ground state ($T=0$); (d)–(f) refer to the low temperature $\beta=10$.

chain by the $\cos(2\kappa)$ term. That term has important consequences, which we explore by generalizing the work of Taylor and Müller²³ on conventional XY chains.

We start with the high-temperature limit $T \rightarrow \infty$. A two-fermion dynamic quantity (2.4) may have a nonzero value at a point (κ, ω) in the wave vector–frequency plane (we assume $\omega \geq 0$, $-\pi \leq \kappa < \pi$) if

$$\omega = E(\kappa_1, \kappa_2) = -\Lambda_{\kappa_1} + \Lambda_{\kappa_2}, \quad \kappa = -\kappa_1 + \kappa_2 [\text{mod}(2\pi)],$$

$$\Lambda_{\kappa} = J \cos \kappa - \frac{K}{2} \cos(2\kappa) + \Omega, \quad (3.1)$$

where $-\pi \leq \kappa_1 < \pi$. We rewrite the function $E(\kappa_1, \kappa_1 + \kappa)$ in the form

$$E(\kappa_1, \kappa_1 + \kappa) = 2 \sin \frac{\kappa}{2} \sin \left(\frac{\kappa}{2} + \kappa_1 \right) \times \left[-J + 2K \cos \frac{\kappa}{2} \cos \left(\frac{\kappa}{2} + \kappa_1 \right) \right] \quad (3.2)$$

and solve the equation $\partial E(\kappa_1, \kappa_1 + \kappa) / \partial \kappa_1 = 0$ with respect to κ_1 or, more precisely, with respect to $x = \cos(\kappa/2 + \kappa_1)$ to find

$$x^{\pm} = \frac{J}{8K \cos \frac{\kappa}{2}} \pm \sqrt{\left(\frac{J}{8K \cos \frac{\kappa}{2}} \right)^2 + \frac{1}{2}}. \quad (3.3)$$

For $|K/J| < 1/2$, there is only one pair of κ_1 that solves Eq. (3.3) and fulfills the condition $|x| \leq 1$, which thus yield a stationary point of the function $E(\kappa_1, \kappa_1 + \kappa)$. That pair is given by $\bar{\kappa}_1^- = \arccos x^- - \kappa/2$ and $\bar{\kappa}_1^+ = -\arccos x^- - \kappa/2$ for $JK > 0$ and by $\bar{\kappa}_1^+ = \arccos x^+ - \kappa/2$ and $\bar{\kappa}_1^- = -\arccos x^+ - \kappa/2$ for $JK < 0$. In the opposite case $|K/J| > 1/2$, there are two such pairs, $\bar{\kappa}_1^- = \arccos x^- - \kappa/2$, $\bar{\kappa}_1^+ = -\arccos x^- - \kappa/2$ and $\bar{\kappa}_1^+ = \arccos x^+ - \kappa/2$, $\bar{\kappa}_1^- = -\arccos x^+ - \kappa/2$. As a result, the upper boundary $\omega_u(\kappa)$ of the two-fermion excitation continuum is given by

$$\Omega_-(\kappa) = |E(\bar{\kappa}_1^-, \bar{\kappa}_1^+ + \kappa)|, \quad JK > 0 \quad (3.4)$$

or

$$\Omega_+(\kappa) = |E(\bar{\kappa}_1^+, \bar{\kappa}_1^+ + \kappa)|, \quad JK < 0. \quad (3.5)$$

Note that for $|K/J| > 1/2$, the first derivative of $E(\kappa_1, \kappa_1 + \kappa)$ with respect to κ_1 is also zero along $\Omega_+(\kappa) < \Omega_-(\kappa) = \omega_u(\kappa)$ for $JK > 0$ or along $\Omega_-(\kappa) < \Omega_+(\kappa) = \omega_u(\kappa)$ for $JK < 0$.

Due to the presence of a two-particle density of states, the two-fermion dynamic quantities (2.1) and (2.4) may exhibit a van Hove singularity along the lines

$$\omega_s(\kappa) = \{\Omega_-(\kappa), \Omega_+(\kappa)\}, \quad (3.6)$$

or, more precisely, along $\Omega_-(\kappa)$ [$\Omega_+(\kappa)$] if $JK > 0$ [$JK < 0$] for $|K/J| < 1/2$ and along both lines $\Omega_-(\kappa)$ and $\Omega_+(\kappa)$ for $|K/J| > 1/2$. Thus, a sufficiently strong three-site interaction K increases the number of van Hove singularities. This is nicely seen in Fig. 4 (and also in Fig. 5) where the two-fermion dynamic structure factors for $J=1$ and $K=2.5$ at $T \rightarrow \infty$ are plotted. [Recall that $B_{zz}(\kappa_1, \kappa_2) = 1$ and therefore, Fig. 4(a) with grayscale plot for $S_{zz}(\kappa, \omega)$ most transparently demonstrates a different (low-frequency) line of van Hove singularities emerging for $|K/J| > 1/2$.]

Interestingly, in addition to the conventional inverse square-root van Hove singularity, a singularity with exponent $-2/3$ may occur as $|K/J| > 1/2$. In fact, by plotting $\partial^2 E(\kappa_1, \kappa_1 + \kappa) / \partial \kappa_1^2|_{\kappa_1 = \bar{\kappa}_1^\pm}$ vs κ , we note that $\partial^2 E(\kappa_1, \kappa_1 + \kappa) / \partial \kappa_1^2|_{\kappa_1 = \bar{\kappa}_1^\pm} = 0$ for $\kappa = \kappa^\diamond$, which satisfies $x^+ = 1$ and $JK > 0$ (or $x^- = -1$ and $JK < 0$). A similar analysis of $\partial^3 E(\kappa_1, \kappa_1 + \kappa) / \partial \kappa_1^3|_{\kappa_1 = \bar{\kappa}_1^\pm}$ vs κ shows that $\partial^3 E(\kappa_1, \kappa_1 + \kappa) / \partial \kappa_1^3|_{\kappa_1 = \bar{\kappa}_1^\pm} \neq 0$ for $\kappa = \kappa^\diamond$. Moreover, we find that $E(\kappa_1, \kappa_1 + \kappa) = 0$ for these values of κ and κ_1 . This immediately implies that $S_f(\kappa^\diamond, \epsilon) \propto \epsilon^{-2/3}$, $\epsilon \rightarrow +0$. In Fig. 5, we demonstrate potential van Hove singularities of the two-fermion dynamic structure factors. In particular, we illustrate the van Hove singularity with exponent $-2/3$ for $J=1$ and $K=2.5$. By solving equation $x^+ = 1$ [Eq. (3.3)] with respect to κ , we find $\kappa^\diamond \approx 2.738\ 876\ 81$. The frequency profiles around this value of

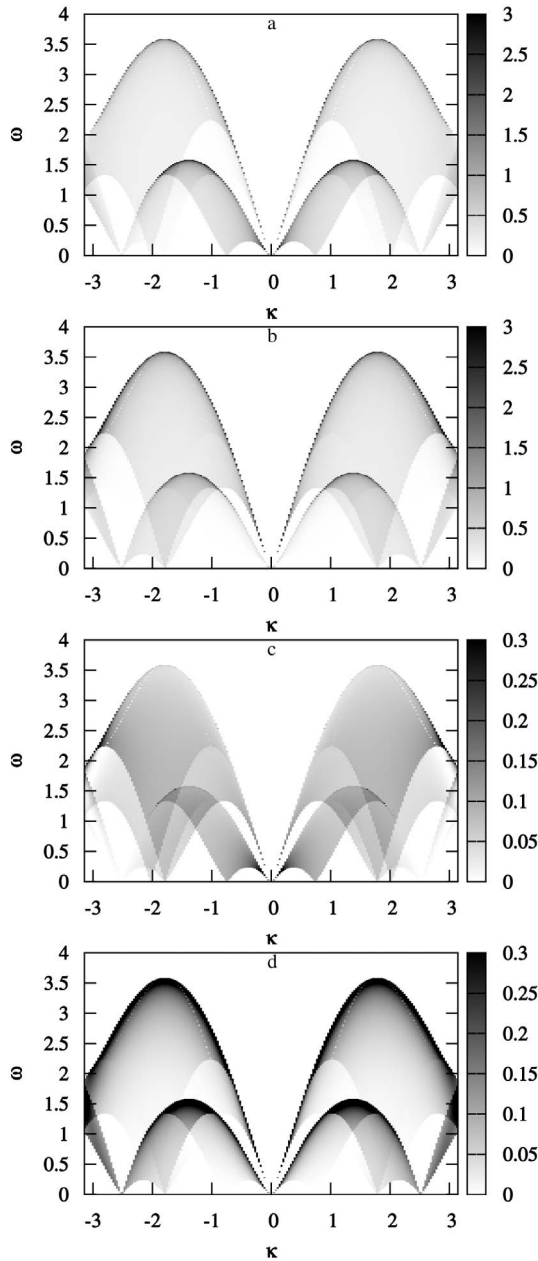


FIG. 3. Two-fermion dynamic structure factors (a) $S_J(\kappa, \omega)$, (b) $S_D(\kappa, \omega)$, (c) $S_K(\kappa, \omega)$, and (d) $S_E(\kappa, \omega)$ for the model (1.1) with $J=1$, $D=E=0$, $K=2.5$, and $\Omega=0$ at $T=0$.

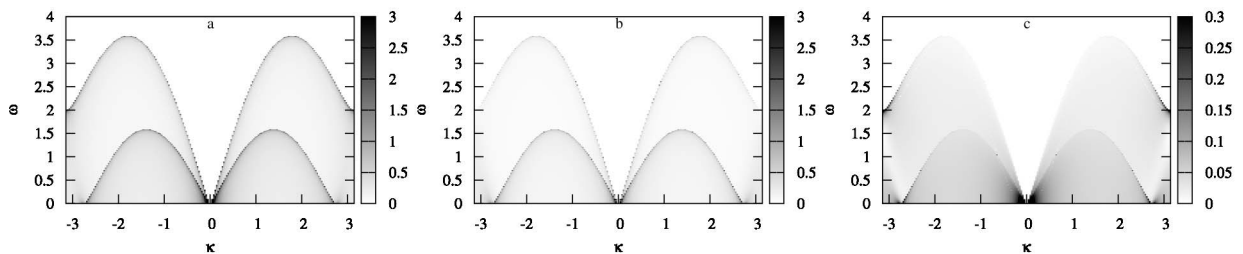


FIG. 4. Two-fermion dynamic structure factors (a) $S_{zz}(\kappa, \omega)$, (b) $S_J(\kappa, \omega)$, and (c) $S_K(\kappa, \omega)$ for the model (1.1) with $J=1$, $D=E=0$, and $K=2.5$ at $T \rightarrow \infty$. Note that for an infinite temperature, the two-fermion dynamic structure factors are field independent.

the wave vector clearly show two types of van Hove singularity, i.e., with exponent $-1/2$ [in most cases, when $\omega \rightarrow \omega_s(\kappa) - \epsilon$, e.g., the dotted and solid lines in Figs. 5(b) and 5(c)] and with exponent $-2/3$ [only when $\kappa = \kappa^\diamond$ and $\omega \rightarrow \epsilon$, e.g., the dashed lines in Figs. 5(b) and 5(c)].

We consider now the case of zero temperature $T=0$ when the Fermi functions entering the function $C(\kappa_1, \kappa_2)$ in Eq. (2.4) become extremely important. They imply that in the ground state, we have to require, in addition to Eq. (3.1), $\Lambda_{\kappa_1} \leq 0$ and $\Lambda_{\kappa_2} \geq 0$. We first consider the case $|K/J| < 1/2$. By plotting the dependence of $E(\kappa_1, \kappa_1 + \kappa)C(\kappa_1, \kappa_1 + \kappa)$ on κ_1 we find that the two characteristic curves, $\Lambda_{\kappa_1 + \kappa}$ with κ_1 satisfying $\Lambda_{\kappa_1} = 0$ [or $E(\kappa_1, \kappa_1 + \kappa)$ with κ_1 satisfying $\Lambda_{\kappa_1} = 0$] and $-\Lambda_{\kappa_1}$ with κ_1 satisfying $\Lambda_{\kappa_1 + \kappa} = 0$ [or $E(\kappa_1, \kappa_1 + \kappa)$ with κ_1 satisfying $\Lambda_{\kappa_1 + \kappa} = 0$], play a special role. By solving the equation $\Lambda_k = 0$ for k , or more precisely for $y = \cos k$, we find

$$y^\pm = \frac{J}{2K} \pm \sqrt{\frac{J^2}{4K^2} + \frac{\Omega}{K} + \frac{1}{2}}. \quad (3.7)$$

By taking into account that $|y| \leq 1$, we see that for $|K/J| < 1/2$, Eq. (3.7) may yield two k values, $\check{k} = \arccos y^-$, $\check{k} = -\arccos y^-$ (for $JK > 0$) or $\check{k} = \arccos y^+$, $\check{k} = -\arccos y^+$ (for $JK < 0$). For $|K/J| > 1/2$, there may be two such pairs of k , $\check{k} = \arccos y^-$, $\check{k} = -\arccos y^-$ and $\check{k} = \arccos y^+$, $\check{k} = -\arccos y^+$; we will discuss that case later.

For $|K/J| < 1/2$, we consider two characteristic lines

$$\omega_-^+(\kappa) = |\Lambda_{\arccos y^- + \kappa}|, \quad \omega_-^-(\kappa) = |\Lambda_{-\arccos y^- + \kappa}|, \quad JK > 0 \quad (3.8)$$

or

$$\omega_+^+(\kappa) = |\Lambda_{\arccos y^+ + \kappa}|, \quad \omega_+^-(\kappa) = |\Lambda_{-\arccos y^+ + \kappa}|, \quad JK < 0. \quad (3.9)$$

The smaller one of the two values $\omega_-^i(\kappa)$, $i = -, +$ for $JK > 0$ [$\omega_+^i(\kappa)$, $i = -, +$ for $JK < 0$] gives the lower boundary of the ground-state two-fermion excitation continuum $\omega_l(\kappa)$, whereas the other (larger) one gives either the upper boundary of the ground-state two-fermion excitation continuum $\omega_u(\kappa)$ or the middle boundary of the ground-state two-fermion excitation continuum $\omega_m(\kappa)$. The former case occurs if $\bar{\kappa}_1$, which yields $\partial E(\kappa_1, \kappa_1 + \kappa) / \partial \kappa_1|_{\kappa_1 = \bar{\kappa}_1} = 0$ (see above), belongs to the region of κ_1 where $E(\kappa_1, \kappa_1 + \kappa)C(\kappa_1, \kappa_1 + \kappa) = 0$ [as, e.g., seen in Fig. 6(b) for small $|\kappa|$]. In the latter case,

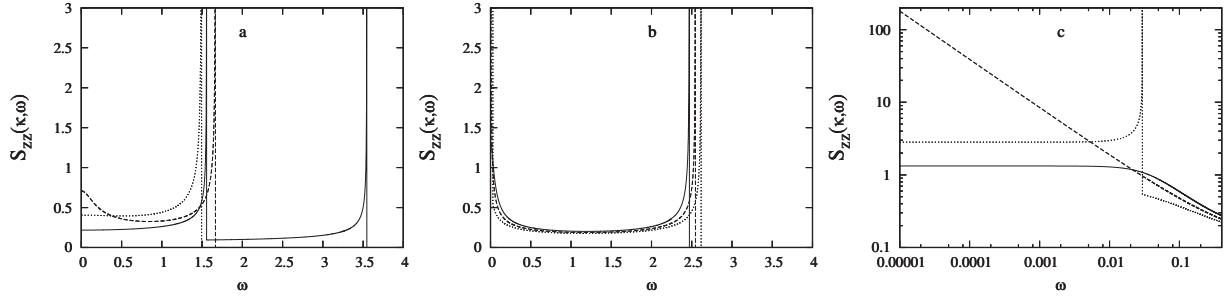


FIG. 5. Different kinds of potential van Hove singularities of the two-fermion dynamic quantities. Frequency profiles of $S_{zz}(\kappa, \omega)$ [i.e., $S_I(\kappa, \omega)$ with $B_I(\kappa_1, \kappa_2)=1$] at $T \rightarrow \infty$ and $J=1$. (a) $\kappa = \pi/2$, $K=0.25$ (dotted line), $K=0.5$ (dashed line), and $K=2.5$ (solid line). [(b) and (c)] $K=2.5$, $\kappa=2.70$ (dotted lines), $\kappa = \kappa^\diamond \approx 2.738\ 876\ 81$ (dashed lines), and $\kappa=2.78$ (solid lines). The initial slope of the dashed line in (c) corresponds to the dependence $\propto \omega^{-2/3}$.

when $\tilde{\kappa}_1$, which yields $\partial E(\kappa_1, \kappa_1 + \kappa) / \partial \kappa_1 |_{\kappa_1 = \tilde{\kappa}_1} = 0$, does belong to the region of κ_1 where $E(\kappa_1, \kappa_1 + \kappa)C(\kappa_1, \kappa_1 + \kappa) \neq 0$, the larger value of $\omega_l^j(\kappa)$, $JK > 0$ [Eq. (3.8)] ($\omega_+^j(\kappa)$, $JK < 0$ [Eq. (3.9)]) gives the middle boundary of the ground-state two-fermion excitation continuum $\omega_m(\kappa)$, whereas the upper boundary $\omega_u(\kappa)$ is given by Eq. (3.4) [Eq. (3.5)]. For the frequencies ω between $\omega_l(\kappa)$ and $\omega_m(\kappa)$ [$\omega_m(\kappa)$ and $\omega_u(\kappa)$], Eq. (2.2) has one solution [two solutions] κ_1^* . Thus, the ground-state $S_I(\kappa, \omega)$ changes by a factor 2 at the middle boundary $\omega_m(\kappa)$.

The soft modes κ_0 can be determined from the equation $\omega_\pm^-(\kappa_0) = 0$, $JK > 0$ [$\omega_\pm^+(\kappa_0) = 0$, $JK < 0$]. Therefore, if $JK > 0$,

$$\kappa_0 = \{0, \pm 2 \arccos y^-\}, \quad y^- > 0,$$

$$\kappa_0 = \{0, \mp 2 \arccos y^- \pm 2\pi\}, \quad y^- < 0 \quad (3.10)$$

or, if $JK < 0$,

$$\kappa_0 = \{0, \pm 2 \arccos y^+\}, \quad y^+ > 0,$$

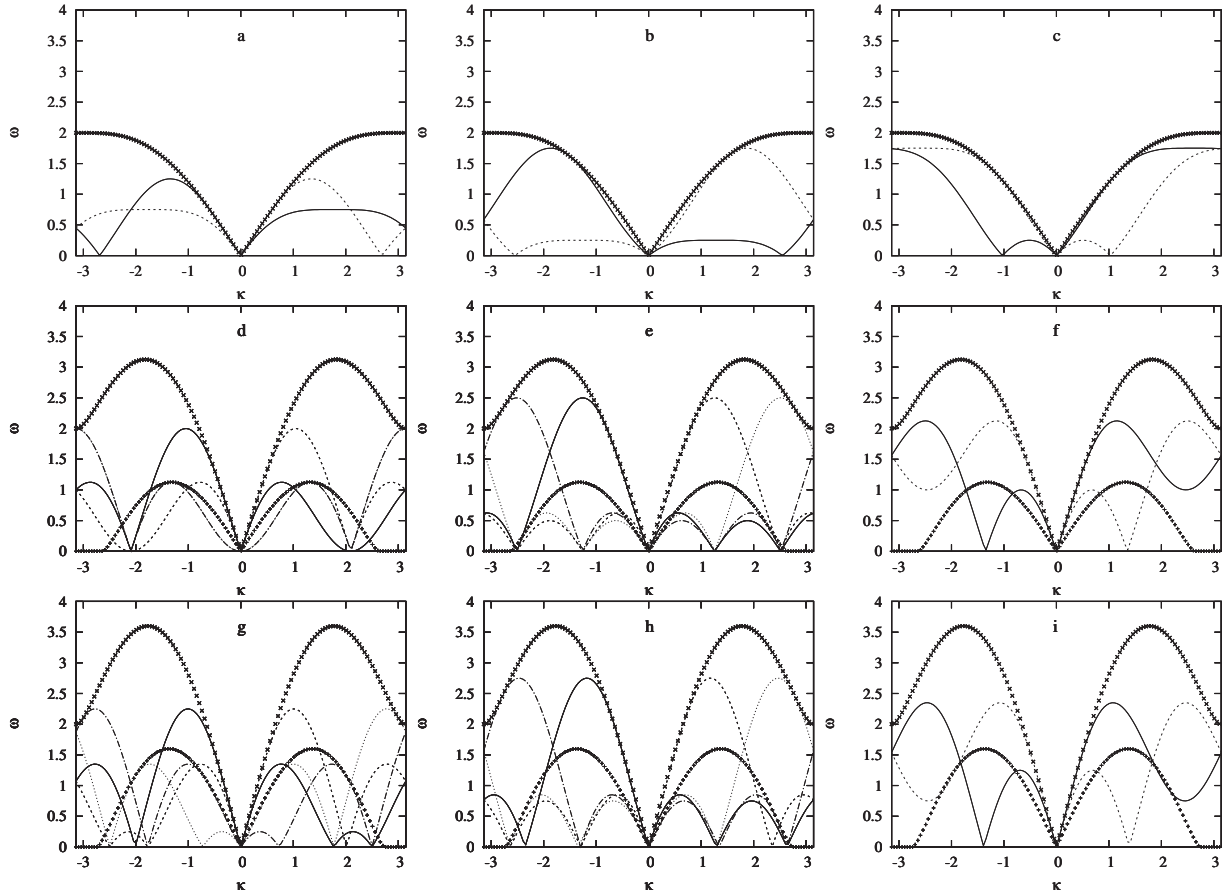


FIG. 6. Characteristic lines of the two-fermion excitation continuum. We assume $J=1$ and $K=0.5$, (a) $\Omega=0$, (b) $\Omega=-0.5$, (c) $\Omega=1$; $K=2$, (d) $\Omega=0$, (e) $\Omega=-0.5$, (f) $\Omega=1$; and $K=2.5$, (g) $\Omega=0$, (h) $\Omega=-0.5$, (i) $\Omega=1$. \times and $+$ symbols correspond to $\Omega_-(\kappa)$ and $\Omega_+(\kappa)$, respectively. Solid, dashed, dash-dotted, and dotted lines correspond to $\omega_+^-(\kappa)$, $\omega_-^-(\kappa)$, $\omega_+^+(\kappa)$, and $\omega_-^+(\kappa)$, respectively. [(a), (d), and (g) can be compared to Figs. 2(a)–2(c).]

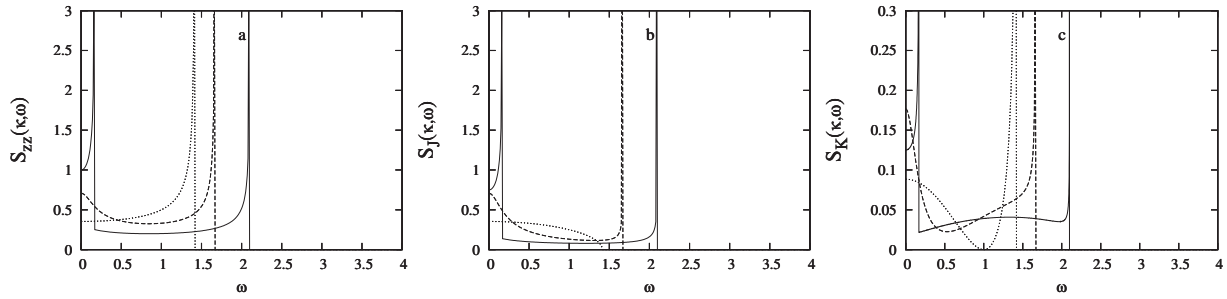


FIG. 7. An illustration of the role of B functions. (a) $S_{zz}(\pi/2, \omega)$, (b) $S_J(\pi/2, \omega)$, and (c) $S_K(\pi/2, \omega)$ at $T \rightarrow \infty$. $J=1$, $K=0$ (dotted lines), $K=0.5$ (dashed lines), and $K=1$ (solid lines).

$$\kappa_0 = \{0, \mp 2 \arccos y^{\pm} \pm 2\pi\}, \quad y^{\pm} < 0. \quad (3.11)$$

We now turn to the case $|K/J| > 1/2$. As already mentioned, Eq. (3.7) may yield two pairs of k , $\check{k} = \arccos y^-$, $\check{k} = -\arccos y^-$ and $\check{k} = \arccos y^+$, $\check{k} = -\arccos y^+$, and, therefore, all four characteristic lines in the κ - ω plane, $\omega^{\pm}(\kappa)$, $\omega_+^+(\kappa)$, and $\omega_+^-(\kappa)$ given by Eqs. (3.8) and (3.9), come into play simultaneously. Thus, as $|K|$ exceeds $|J|/2$, an “extra” ground-state two-fermion excitation continuum emerges. Its lower boundary and upper on middle boundary are given by formulas (3.8) and (3.9) [in the case when Eqs. (3.8) and (3.9) give the middle boundary, the upper boundary is given by one of the formulas in Eqs. (3.4) and (3.5)]. The number of soft modes increases but cannot exceed 9.

In the vicinity of a soft mode κ_0 , the lower boundary of the two-fermion continuum in most cases displays a “V” shape, i.e., it is proportional to $|\kappa - \kappa_0|$. However, it is worth noting that a parabolic shape $\propto (\kappa - \kappa_0)^2$ is also possible for suitable parameter combinations. To see this, we recall that the lower boundary is basically determined by the equation $\Lambda_k = 0$ with $\Lambda_k = J \cos k - (K/2) \cos(2k) + \Omega$. For the conventional XX chain ($K=0$) in a transverse field Ω , we see that at the critical field values $\Omega = \pm |J|$ the dispersion $\Lambda_k \propto (k - k_0)^2$, with a corresponding parabolic shape of the lower continuum boundary near a soft mode at κ_0 . (This can be seen, e.g., in Fig. 11f of Ref. 24.) At the critical field, the nature of the ground state of the XX chain changes from partially filled to completely filled or completely empty in terms of Jordan–Wigner fermions. For nonzero K , the $\cos(2k)$ term may generate additional maxima or minima in Λ_k . That implies the emergence of additional critical field values, at which k regions near the additional minima or maxima of Λ_k open or close for occupation by Jordan–Wigner fermions. These critical values correspond to the lines separating different ground-state phases in Fig. 1. Along these lines, we expect a parabolic behavior of the lower two-fermion continuum boundary [see, e.g., Figs. 2(b) and 2(d)–2(f)].

By summarizing this part, we report in Fig. 6 all of the characteristic lines of the two-fermion excitation continuum discussed above. In these plots, symbols correspond to $\Omega_-(\kappa)$ (x symbols) and $\Omega_+(\kappa)$ (+ symbols), whereas lines correspond to $\omega_+^-(\kappa)$ (solid line), $\omega_+^-(\kappa)$ (dashed line), $\omega_+^+(\kappa)$ (dash-dotted line), and $\omega_+^+(\kappa)$ (dotted line). For $|K/J| < 1/2$, only three characteristic lines are relevant, but if $|K/J| > 1/2$, all six lines are relevant. These lines are important not only for understanding the distribution of the two-fermion dynamic

structure factors $S_I(\kappa, \omega)$ [Eqs. (2.1) and (2.4)] over the κ - ω plane (see grayscale plots in Figs. 2–4) but also for many-fermion dynamic structure factors [like $S_{xx}(\kappa, \omega)$] at low temperatures, as will be discussed in Sec. IV (see grayscale plots in Fig. 10).

Finally, we discuss some specific properties of the two-fermion dynamic structure factors (2.4) controlled by different B functions. By comparing different panels in Figs. 3 and 4, we observe a number of small but definite differences for the detailed distributions of $S_I(\kappa, \omega)$ over the κ - ω plane.

To be specific, we may focus on the dynamic dimer structure factor $S_J(\kappa, \omega)$. It is known that $S_J(\kappa, \omega)$ does not diverge along the upper boundary due to $B_J(\kappa_1, \kappa_2)$ for the conventional XX chain, i.e., when $K=0$ (see, e.g., Ref. 25 and references therein). This can also be seen in Fig. 7(b), where the dotted line corresponds to $K=0$. This changes, however, if $K \neq 0$: the dynamic dimer structure factor exhibits a van Hove singularity along the upper boundary [the dashed and solid lines in Fig. 7(b)], which indicates the presence of nonzero three-site interactions.

Next we may consider $S_K(\kappa, \omega)$. As can be seen in Figs. 4(c) and 7(c), the van Hove singularity at the upper boundary becomes less distinctive as K increases. To explain this, we introduce the notation $x = \cos(\kappa/2 + \kappa_1)$ and rewrite $\partial E(\kappa_1, \kappa_1 + \kappa) / \partial \kappa_1$ [Eq. (3.2)] as $2 \sin(\kappa/2) [2K \cos(\kappa/2)(2x^2 - 1) - Jx]$, whereas $B_K(\kappa_1, \kappa_1 + \kappa)$ [Eq. (2.4)] as $(1/4)(2x^2 - 1)^2$. In the vicinity of the upper boundary, the denominator in Eq. (2.4) for $S_K(\kappa, \omega)$ tends to zero; however, in the limit $K \rightarrow \infty$, the numerator in Eq. (2.4) for $S_K(\kappa, \omega)$ becomes proportional to the denominator squared, which makes the fraction equal to zero. Thus, for any finite large K , the van Hove singularity at the upper boundary does exist (although with increasing K , it is harder to numerically find it) and it disappears only in the limit $K \rightarrow \infty$.

IV. MANY-FERMION DYNAMIC QUANTITIES

In this section, we discuss many-fermion dynamic quantities, fixing for concreteness our attention to the xx dynamic structure factor $S_{xx}(\kappa, \omega)$. First, we report two analytical results referring to the high-temperature limit and to the zero-temperature strong-field regime, respectively, and then we turn to high precision numerical data for arbitrary values of temperature and the Hamiltonian parameters.

We first consider the xx two-spin time-dependent correlation function $\langle S_j^x(t) S_{j+n}^x \rangle$ at $T \rightarrow \infty$. Since the Zeeman term

commutes with the Hamiltonian of the considered model (1.1) and, in the high-temperature limit, $\exp(-\beta H) \rightarrow 1$ and, consequently, the averages of spin operators are zero, we can easily extract the dependence on the transverse field Ω as follows:

$$\langle s_j^x(t) s_{j+n}^x \rangle = \cos(\Omega t) \langle s_j^x(t) s_{j+n}^x \rangle |_{\Omega=0}. \quad (4.1)$$

Thus, we can proceed assuming $\Omega=0$. Next, we substitute into the spin correlation function on the right hand side in Eq. (4.1) a short-time expansion³³ $s_j^x(t) = s_j^x + i[H, s_j^x]t - (1/2)[H, [H, s_j^x]]t^2 + \dots$ and, after simple but tedious calculations, we find

$$4 \langle s_j^x(t) s_{j+n}^x \rangle |_{\Omega=0} = \delta_{n,0} \left[1 - \left(\frac{J_{j-1}^2 + J_j^2}{8} + \frac{K_{j-2}^2 + 2K_{j-1}^2 + K_j^2}{32} \right) t^2 + \dots \right], \quad (4.2)$$

where, for generality, we have considered a model with position-dependent couplings. Equation (4.2) is consistent with the Gaussian decay

$$4 \langle s_j^x(t) s_{j+n}^x \rangle = \delta_{n,0} \cos(\Omega t) \exp \left[- \left(\frac{J^2}{4} + \frac{K^2}{8} \right) t^2 \right] \quad (4.3)$$

for the model with position-independent couplings. By using MAPLE codes, we checked that the terms up to t^4 in the short-time expansion for $\langle s_j^x(t) s_{j+n}^x \rangle$, indeed, agree with Eq. (4.3).

Alternative (although not independent) arguments supporting Eq. (4.3) follow Refs. 34 and 35. We examine the continued-fraction coefficients Δ_k of the relaxation function $c^{xx}(z) = 4 \int_0^\infty dt \exp(-zt) \langle s_j^x(t) s_j^x \rangle = 1 / \{z + \Delta_1 / [z + \Delta_2 / (z + \dots)]\}$ at $T \rightarrow \infty$. The sequence of the continued-fraction coefficients Δ_k reflects the time dependence of the associated autocorrelation function and, in particular, when $\Delta_k = k\Delta$, then $4 \langle s_j^x(t) s_j^x \rangle = \exp(-\Delta t^2/2)$. The sequence Δ_k can be determined by the methods elaborated in Ref. 35. We designed a MAPLE program which, in a reasonable amount of time, calculated Δ_k for $k=1, 2, 3, 4$ and confirmed the Gaussian decay (4.3).

Finally, from our calculations, we also find a more general result for the homogeneous model (1.1), which is given by Eq. (4.3) after the substitution $J^2 \rightarrow J^2 + D^2$ and $K^2 \rightarrow K^2 + E^2$.

To summarize, in Fig. 8, we compare analytical predictions according to Eq. (4.3) (symbols) with numerical calculations (lines) (see below) and observe an excellent agreement between both sets of data. Equation (4.3) provides an extension of the well-known result for the conventional transverse XX chain³⁶ for the kind of three-site interactions considered here. The presented arguments in favor of the Gaussian decay (4.3) may be put even on a more rigorous foundation by using the approach elaborated in Ref. 37.

Next, we turn to the zero-temperature strong-field regime. More precisely, we consider the ferromagnetic phase (light) in Fig. 1. In the ferromagnetic phase, the ground state of the spin model is completely polarized, i.e., $|\text{GS}\rangle = |\Pi_n | \downarrow \rangle_n$ ($|\text{GS}\rangle = |\Pi_n | \uparrow \rangle_n$) for positive (negative) Ω , which permits to easily take into account the Jordan-Wigner sign factors en-

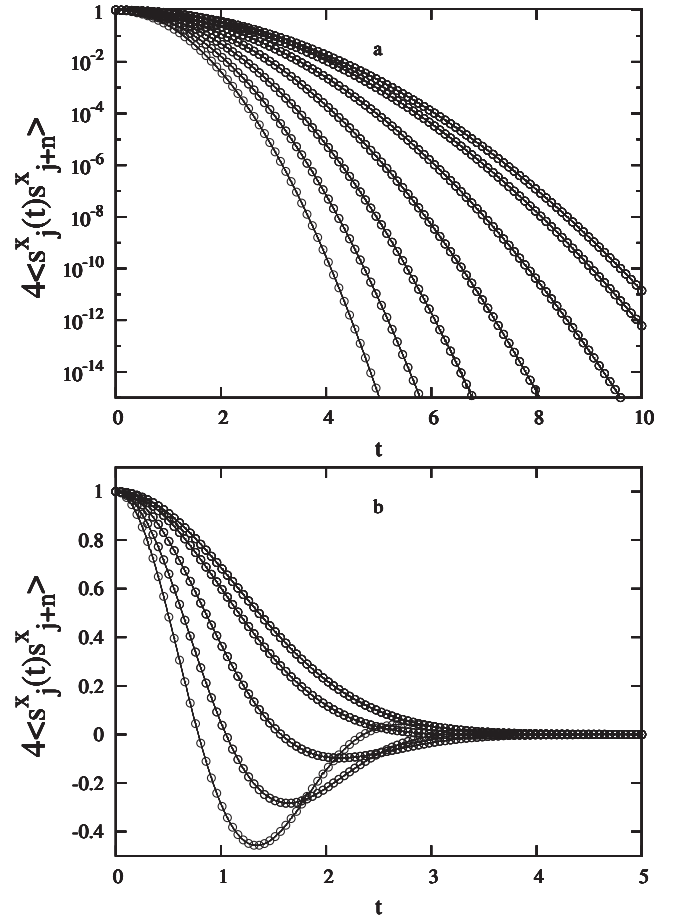


FIG. 8. Time dependence of the xx autocorrelation function in the high-temperature limit ($\beta=0.0001$); $J=1$. (a) $\langle s_j^x(t) s_{j+n}^x \rangle$ at $\Omega=0$ and $K=0, 0.5, 1, 1.5, 2, 2.5,$ and 3 (from top to bottom). (b) $\langle s_j^x(t) s_{j+n}^x \rangle$ at $K=1$ and $\Omega=0, 0.5, 1, 1.5,$ and 2 (from top to bottom). Symbols correspond to Eq. (4.3); lines correspond to numerical data obtained for $N=400$ and $j=41$.

tering the formula for $\langle s_j^x(t) s_{j+n}^x \rangle$.³⁸ By assuming, for example, $|\text{GS}\rangle = |\Pi_n | \downarrow \rangle_n$ (light region in the upper half-plane in Fig. 1), we immediately get

$$4 \langle s_j^x(t) s_{j+n}^x \rangle = \frac{1}{N} \sum_{\kappa} \exp[i(\kappa n - \Lambda_{\kappa} t)] \xrightarrow{N \rightarrow \infty} \frac{1}{2\pi} \int_{-\pi}^{\pi} d\kappa \exp[i(\kappa n - \Lambda_{\kappa} t)], \quad (4.4)$$

with $\Lambda_{\kappa} = J \cos \kappa - (K/2) \cos(2\kappa) + \Omega > 0$. For $|\text{GS}\rangle = |\Pi_n | \uparrow \rangle_n$ (light region in the lower half-plane in Fig. 1), we have

$$4 \langle s_j^x(t) s_{j+n}^x \rangle = \frac{1}{N} \sum_{\kappa} \exp\{-i[(\kappa \mp \pi)n - \Lambda_{\kappa} t]\} \xrightarrow{N \rightarrow \infty} \frac{1}{2\pi} \int_{-\pi}^{\pi} d\kappa \times \exp\{-i[(\kappa \mp \pi)n - \Lambda_{\kappa} t]\}, \quad (4.5)$$

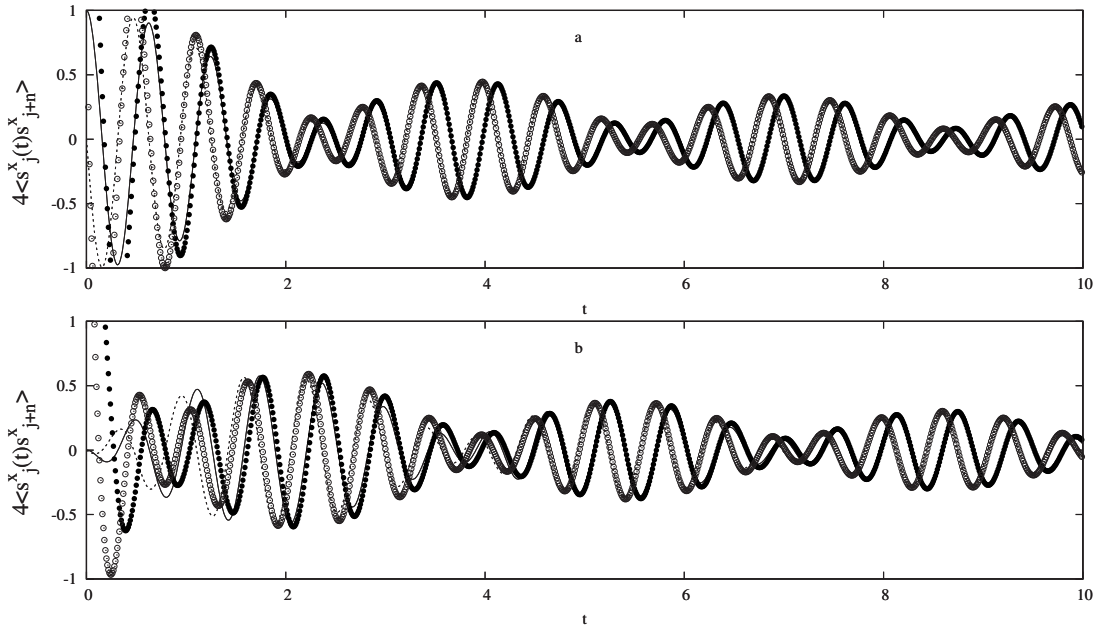


FIG. 9. Time dependence of $\langle s_j^x(t)s_{j+n}^x \rangle$ [(a) $n=0$; (b) $n=1$] in the low-temperature limit ($\beta=100$); $J=1$, $K=0.25$, and $\Omega=10$. Lines correspond to numerical data for $N=400$ and $j=101$. Symbols correspond to the long-time asymptotics given by Eq. (A6). (We notice that the asymptotic becomes accurate already for short times.) Solid (dashed) lines or filled (empty) symbols refer to the real (imaginary) part of $\langle s_j^x(t)s_{j+n}^x \rangle$.

with $\Lambda_\kappa = J \cos \kappa - (K/2)\cos(2\kappa) + \Omega < 0$. Equations (4.4) and (4.5) contain the result for the conventional transverse XX chain,³⁸ $4\langle s_j^x(t)s_{j+n}^x \rangle = \exp(-i|\Omega|t)(-i)^n J_n(Jt)$, where $J_n(z)$ is the Bessel function of the first kind.³⁹ Some further properties of $\langle s_j^x(t)s_{j+n}^x \rangle$ are collected in the Appendix. We only notice here that in the regime considered, the xx time-dependent correlation function oscillates, with the envelope decaying proportional to $t^{-1/2}$ as $t \rightarrow \infty$ for $|K/J| \neq 1/2$ or proportional to $t^{-1/4}$ for $|K/J|=1/2$ [see Eqs. (A6)–(A8) and Fig. 9].

Equations (4.3)–(4.5) immediately yield the xx dynamic structure factor (1.8). In the high-temperature limit, we have

$$S_{xx}(\kappa, \omega) = \frac{\sqrt{\pi}}{4\sqrt{J^2 + \frac{K^2}{2}}} \left[\exp\left(-\frac{(\omega - \Omega)^2}{J^2 + \frac{K^2}{2}}\right) + \exp\left(-\frac{(\omega + \Omega)^2}{J^2 + \frac{K^2}{2}}\right) \right], \quad (4.6)$$

i.e., the xx dynamic structure factor displays a κ -independent Gaussian ridge centered at frequency $|\Omega|$ with the width controlled by interspin interactions. In the zero-temperature strong-field regime, we have

$$S_{xx}(\kappa, \omega) = \frac{\pi}{2} \delta[\omega - \omega^*(\kappa)],$$

$$\omega^*(\kappa) = \begin{cases} |\Omega| + J \cos \kappa - \frac{K}{2} \cos(2\kappa), & \Omega > 0 \\ |\Omega| + J \cos \kappa + \frac{K}{2} \cos(2\kappa), & \Omega < 0, \end{cases} \quad (4.7)$$

i.e., the xx dynamic structure factor displays a δ peak along the line $\omega^*(\kappa)$ [Eq. (4.7)] in the κ - ω plane. Interestingly, if $K \neq 0$, the symmetry of Eq. (4.7) with respect to the change $\Omega \rightarrow -\Omega$ is broken, which is in agreement with the ground-state phase diagram shown in Fig. 1.

We turn next to the case of arbitrary values of temperature and the Hamiltonian parameters. In this case, we numerically calculate the xx dynamic structure factor. The numerical approach for calculating dynamic quantities was explained in detail earlier.^{24,40} To calculate $\langle s_j^x(t)s_{j+n}^x \rangle$, we express the spin operators s^x entering this quantity in terms of the Fermi operators $c_\kappa, c_\kappa^\dagger$ according to Eqs. (1.4) and (1.6), obtaining as a result an average of a product of a large number of Fermi operators attached not only to the sites j and $j+n$ but to two strings of sites extending to the site $j=1$. We apply the Wick–Bloch–de Dominicis theorem and present the result as the Pfaffian of the $2(2j+n-1) \times 2(2j+n-1)$ antisymmetric matrix constructed from the known elementary contractions (only these quantities are influenced by the existence of three-site interactions). Finally, we numerically evaluate the Pfaffians, obtaining as a result the desired xx time-dependent spin correlation function. To get $S_{xx}(\kappa, \omega)$ [Eq. (1.8)], we numerically perform the integration over time t and then the summation over n . Typically, we take $N=400$, assume $j=41$, and calculate $\langle s_j^x(t)s_{j+n}^x \rangle$ for n up to $n_{\max}=100$ in the time range up to $t_{\max}=100$. (However, for large Ω , we assume $j=81$, $n_{\max}=100$, and $t_{\max}=200$, whereas for $\beta=0.1$, it

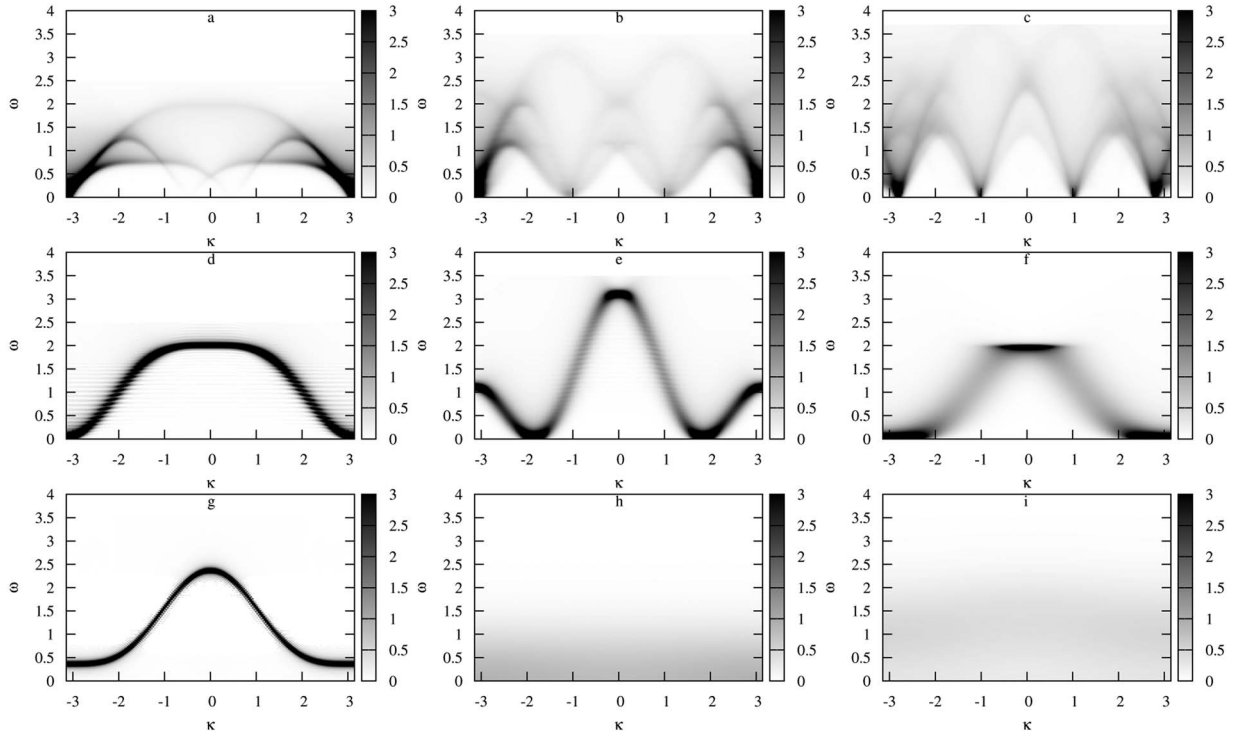


FIG. 10. $S_{xx}(\kappa, \omega)$ for the model (1.1) with $J=1$ and $D=E=0$; (a) $K=0.5$, $\Omega=0$; (b) $K=2$, $\Omega=0$; (c) $K=2.5$, $\Omega=0$; (d) $K=0.5$, $\Omega=1.25$; (e) $K=2$, $\Omega=-1.125$; (f) $K=0.5$, $\Omega=-0.75$; and (g) $K=0.5$, $\Omega=-1.125$ (for this set of parameters, we assume $\epsilon=0.02$; see the main text) at low temperature $\beta=20$. (h) and (i) correspond to the high-temperature limit; $\beta=0.1$, $K=0.5$, and (h) $\Omega=0$ or (i) $\Omega=-1.125$.

is sufficient to take $j=41$, $n_{\max}=50$, and $t_{\max}=50$.) In the low-temperature strong-field regime, the xx time-dependent spin correlation functions display long-time oscillations, which lead to evident problems with integrating over time; therefore, in this case [in fact, only for the set of parameters corresponding to Fig. 10(g)], we introduce under the integral in Eq. (1.8) an auxiliary damping factor $\exp(-\epsilon|t|)$, where ϵ is a small positive number. We examine in detail different types of finite size effects^{24,40} to be sure that our results for $S_{xx}(\kappa, \omega)$ refer to the thermodynamic limit. In Fig. 10, we demonstrate the results for the xx dynamic structure factors for a set of parameters that is in correspondence with the one used in Figs. 2(a)–2(f) and the analytical predictions (4.6) and (4.7) [Figs. 2(g)–2(i)].

We start discussing the results obtained for $S_{xx}(\kappa, \omega)$ from the case of low temperatures. Although $S_{xx}(\kappa, \omega)$ is a many-fermion quantity and, therefore, is not restricted to a certain region in the κ - ω plane, it is mostly concentrated along certain lines in the κ - ω plane, which roughly correspond to the characteristic lines of the two-fermion excitation continuum discussed in Sec. III [cf. Figs. 10(a)–10(c) with Figs. 2(a)–2(c) and Figs. 6(a), 6(d), and 6(g) as well as Figs. 10(d)–10(f) with Figs. 2(d)–2(f)]. For example, for $J=1$, $K=0.5$, and $\Omega=0$ [Fig. 10(a)] $S_{xx}(\kappa, \omega)$ is accumulated along the three lines in the κ - ω plane, $\Omega_-(\kappa)$ [Eq. (3.4)] and $\omega_{\pm}^{\pm}(\kappa)$ [Eq. (3.8)], shifted along the κ axis by π . Although the important role of the two-fermion excitations for the low-temperature many-fermion dynamic quantities such as $S_{xx}(\kappa, \omega)$ was noted several times earlier, we still do not have a simple explanation for that fact. On the other hand, Figs. 10(d)–10(g) demonstrate the development toward the zero-temperature strong-field result (4.7).

As temperature increases, the role of the two-fermion excitations diminishes and, in the high-temperature limit, many-fermion excitations produce the κ -independent Gaussian decay (4.6) [cf. Figs. 10(h) and 10(i) to Figs. 10(a) and 10(g), respectively].

V. CONCLUSIONS

In conclusion, we have examined several dynamic structure factors of the spin- $\frac{1}{2}$ transverse XX chain with $(XZX + YZY)$ -type three-site interactions. These three-site interactions essentially enrich the ground-state phase diagram of the spin model which, may show two different spin liquid phases (spin liquid I and spin liquid II) in addition to the ferromagnetic phase. We have explicitly calculated several dynamic structure factors [with the transverse dynamic structure factor $S_{zz}(\kappa, \omega)$ and the dimer dynamic structure factor $S_f(\kappa, \omega)$ among them], which are exclusively governed by two-fermion (particle-hole) excitations. We have discussed in some detail the properties of the two-fermion excitation continuum, determining its boundaries, soft modes, and exponents of van Hove singularities.⁴¹ We have also discussed some specific features of different two-fermion dynamic structure factors. Our analysis of many-fermion dynamic structure factors is restricted to the xx dynamic structure factor $S_{xx}(\kappa, \omega)$. For this quantity, we have reported exact analytical results in the high-temperature and zero-temperature strong-field limits and precise numerical results for other sets of parameters. The three-site interactions introduced left a number of signatures in the dynamic quantities, which produced an extra two-fermion excitation continuum, a van

Hove singularity with exponent $2/3$, or a singularity of the dimer structure factor along the upper boundary of the two-fermion excitation continuum. In the presence of three-site interactions, the symmetry of the xx dynamic structure factor in the zero-temperature strong-field regime with respect to the change $\Omega \rightarrow -\Omega$ is broken.

We emphasize that the advantage of the model considered is its exact solvability, that means, in particular, the possibility to accurately calculate various dynamic quantities. On the other hand, although there are some examples of real-life systems that can be modeled as spin- $\frac{1}{2}$ XX chains (see, e.g., Ref. 42), the three-site interactions introduced are of a rather special kind, however, the reported results may serve to test other (approximate) techniques used to study more realistic models, e.g., with next-nearest-neighbor interactions or with four-site interactions. Moreover, our results on dynamics may be used to discuss the effects of stationary energy fluxes in quantum spin chains. Thus, in Ref. 3(c), the transverse (zz) dynamic structure factor for a model with $D=K=0$ was discussed in relation to possible experimental observation of energy-current carrying states in quantum spin chain compounds.

ACKNOWLEDGMENTS

This research was supported by a NATO collaborative linkage grant, Reference No. CBP.NUKR.CLG 982540, project ‘‘Dynamic Probes of Low-Dimensional Quantum Magnets.’’ J.S. acknowledges the kind hospitality of ICMP, L’viv, where part of this work was done. The authors thank U. L ow for a critical reading of the manuscript.

APPENDIX: TIME-DEPENDENT xx SPIN CORRELATIONS IN THE ZERO-TEMPERATURE STRONG-FIELD REGIME

We can rewrite Eq. (4.4) [$\Omega > 0$ (Ref. 43)] as follows:

$$4\langle s_j^x(t)s_{j+n}^x \rangle = \exp\left[-i\left(\Omega + \frac{K}{2}\right)t\right]\mathcal{L}_n, \quad (\text{A1})$$

with

$$\mathcal{L}_n \equiv \frac{1}{\pi} \int_0^\pi d\kappa \cos(\kappa n) \exp[-it(J \cos \kappa - K \cos^2 \kappa)]. \quad (\text{A2})$$

The function \mathcal{L}_n introduced in Eq. (A2) for even n can be expressed in terms of the function $\Phi_3(\beta, \gamma, x, y)$ (see Sec. 5.7.1 in Ref. 44) as follows:

$$\begin{aligned} \mathcal{L}_0 &= \exp(iKt) \Phi_3\left(\frac{1}{2}, 1; -iKt, \frac{J^2 t^2}{4}\right), \\ \mathcal{L}_{2m} &= \exp(iKt) \sum_{l=0}^m (-1)^l \frac{m\Gamma(m+l)}{\Gamma(m-l+1)\Gamma^2(l+1)} \\ &\quad \times \Phi_3\left(l + \frac{1}{2}, l+1; -iKt, \frac{J^2 t^2}{4}\right), \end{aligned} \quad (\text{A3})$$

where $\Gamma(n)$ is the gamma function.

We notice that, in the case $K=0$,

$$\mathcal{L}_n = (-i)^n J_n(Jt), \quad (\text{A4})$$

whereas in the case $J=0$,

$$\mathcal{L}_n = \begin{cases} \exp\left(i\frac{Kt}{2}\right) i^m J_n\left(\frac{Kt}{2}\right), & n = 2m \\ 0, & n = 2m + 1, \end{cases} \quad (\text{A5})$$

where $J_n(z)$ is the Bessel function of the first kind.

Finally, we notice that the long-time asymptotics for $\langle s_j^x(t)s_{j+n}^x \rangle$ in the zero-temperature strong-field regime can be accurately calculated by using the stationary phase method.⁴⁵ For $|K/J| < 1/2$, we have

$$\mathcal{L}_n \approx \frac{1}{\sqrt{2\pi|J|t}} \exp(iKt) \left(\frac{\exp\left[-iJt + i\frac{\pi}{4} \operatorname{sgn}(J)\right]}{\sqrt{\left|1 - \frac{2K}{J}\right|}} + \frac{\exp\left[iJt - i\frac{\pi}{4} \operatorname{sgn}(J) + i\pi n\right]}{\sqrt{\left|1 + \frac{2K}{J}\right|}} \right). \quad (\text{A6})$$

For $|K/J| > 1/2$, we have

$$\begin{aligned} \mathcal{L}_n &\approx \frac{1}{\sqrt{2\pi|J|t}} \exp(iKt) \left(\frac{\exp\left[-iJt + i\frac{\pi}{4} \operatorname{sgn}(J-2K)\right]}{\sqrt{\left|1 - \frac{2K}{J}\right|}} + \frac{\exp\left[iJt - i\frac{\pi}{4} \operatorname{sgn}(J+2K) + i\pi n\right]}{\sqrt{\left|1 + \frac{2K}{J}\right|}} \right) \\ &\quad + 2 \frac{\exp\left[-i\left(K + \frac{J^2}{4K}\right)t + i\frac{\pi}{4} \operatorname{sgn}\left(2K - \frac{J^2}{2K}\right)\right]}{\sqrt{\left|\frac{2K}{J} - \frac{J}{2K}\right|}} \cos\left(n \arccos \frac{J}{2K}\right). \end{aligned} \quad (\text{A7})$$

For $|K/J|=1/2$, we have

$$\begin{aligned} \mathcal{L}_n \stackrel{t \rightarrow \infty}{\approx} & (-1)^{(n/2)[1-\text{sgn}(JK)]} \left\{ \frac{\Gamma(\frac{1}{4})}{2\pi(2|J|t)^{1/4}} \exp \left[i \text{sgn}(JK) \left(-\frac{1}{2}Jt + \frac{\pi}{8} \text{sgn}(J) \right) \right] \right. \\ & \left. + \frac{1}{2\sqrt{\pi|J|t}} \exp \left[i \text{sgn}(JK) \left(\frac{3}{2}Jt - \frac{\pi}{4} \text{sgn}(J) \right) + i\pi n \right] \right\}. \end{aligned} \quad (\text{A8})$$

The long-time asymptotic behaviors (A6)–(A8) may emerge already at relatively short times, as can be seen in Fig. 9.

-
- ¹E. Lieb, T. Schultz, and D. Mattis, *Ann. Phys. (N.Y.)* **16**, 407 (1961); S. Katsura, *Phys. Rev.* **127**, 1508 (1962); **129**, 2835 (1963).
- ²K. Yosida, *Theory of Magnetism* (Springer-Verlag, Berlin, 1996); A. H. MacDonald, S. M. Girvin, and D. Yoshioka, *Phys. Rev. B* **37**, 9753 (1988); **41**, 2565 (1990); A. L. Chernyshev, D. Galanakis, P. Phillips, A. V. Rozhkov, and A.-M. S. Tremblay, *ibid.* **70**, 235111 (2004); A. Reischl, E. Müller-Hartmann, and G. S. Uhrig, *ibid.* **70**, 245124 (2004).
- ³T. Antal, Z. Rácz, A. Rákos, and G. M. Schütz, *Phys. Rev. E* **57**, 5184 (1998); **59**, 4912 (1999); Z. Rácz, *J. Stat. Phys.* **101**, 273 (2000).
- ⁴Y. Ogata, *Phys. Rev. E* **66**, 016135 (2002).
- ⁵V. Eisler and Z. Zimborás, *Phys. Rev. A* **71**, 042318 (2005).
- ⁶M. Suzuki, *Phys. Lett.* **34A**, 338 (1971); M. Suzuki, *Prog. Theor. Phys.* **46**, 1337 (1971).
- ⁷A. M. Tselik, *Phys. Rev. B* **42**, 779 (1990).
- ⁸H. Frahm, *J. Phys. A* **25**, 1417 (1992).
- ⁹D. Gottlieb and J. Rössler, *Phys. Rev. B* **60**, 9232 (1999).
- ¹⁰O. Derzhko, J. Richter, and V. Derzhko, *Ann. Phys.* **8**, SI-49 (1999).
- ¹¹I. Titvinidze and G. I. Japaridze, *Eur. Phys. J. B* **32**, 383 (2003).
- ¹²P. Lou, W.-C. Wu, and M.-C. Chang, *Phys. Rev. B* **70**, 064405 (2004).
- ¹³P. Lou, *Phys. Status Solidi B* **241**, 1343 (2004).
- ¹⁴P. Lou, *Phys. Rev. B* **72**, 064435 (2005).
- ¹⁵P. Lou, *Phys. Status Solidi B* **242**, 3209 (2005).
- ¹⁶J. K. Pachos, *Int. J. Quantum Inf.* **4**, 541 (2006).
- ¹⁷M.-F. Yang, *Phys. Rev. A* **71**, 030302(R) (2005).
- ¹⁸J. Zhang, X. Peng, and D. Suter, *Phys. Rev. A* **73**, 062325 (2006).
- ¹⁹P. Lou and J. Y. Lee, *Phys. Rev. B* **74**, 134402 (2006).
- ²⁰C.-s. Yu, H.-s. Song, and H.-t. Cui, arXiv:quant-ph/0611011 (unpublished).
- ²¹A. A. Zvyagin and G. A. Skorobogat'ko, *Phys. Rev. B* **73**, 024427 (2006).
- ²²A. A. Zvyagin, *Phys. Rev. B* **73**, 104414 (2006).
- ²³J. H. Taylor and G. Müller, *Physica A* **130**, 1 (1985), and references therein.
- ²⁴O. Derzhko, T. Krokhmalkii, and J. Stolze, *J. Phys. A* **33**, 3063 (2000).
- ²⁵O. Derzhko, T. Krokhmalkii, J. Stolze, and G. Müller, *Phys. Rev. B* **71**, 104432 (2005).
- ²⁶A. A. Zvyagin, *Phys. Rev. B* **72**, 064419 (2005).
- ²⁷J. H. H. Perk and H. W. Capel, *Phys. Lett.* **58A**, 115 (1976); M. Oshikawa and I. Affleck, *Phys. Rev. Lett.* **79**, 2883 (1997); O. Derzhko, J. Richter, and O. Zaburannyi, *J. Phys.: Condens. Matter* **12**, 8661 (2000); D. N. Aristov and S. V. Maleyev, *Phys. Rev. B* **62**, R751 (2000); M. Bocquet, F. H. L. Essler, A. M. Tselik, and A. O. Gogolin, *ibid.* **64**, 094425 (2001).
- ²⁸S. Sachdev, *Quantum Phase Transitions* (Cambridge University Press, Cambridge, England, 1999).
- ²⁹S. Daul and R. M. Noack, *Phys. Rev. B* **58**, 2635 (1998); **61**, 1646 (2000); G. I. Japaridze, R. M. Noack, D. Baeriswyl, and L. Tincani, *ibid.* **76**, 115118 (2007); S. Nishimoto, K. Sano, and Y. Ohta, arXiv:0710.2274v1 [cond-mat.str-el] (unpublished).
- ³⁰D. N. Zubarev, *Njeravnovjesnaja Statisticheskaja Tjermodynamika* (Nauka, Moskva, 1971) (in Russian); *Nonequilibrium Statistical Thermodynamics* (Consultants Bureau, New York, 1974).
- ³¹T. Krokhmalkii, O. Derzhko, J. Stolze, and T. Verkholyak, *Acta Phys. Pol. A* **113**, 437 (2008).
- ³²Th. Niemejer, *Physica (Amsterdam)* **36**, 377 (1967).
- ³³O. V. Derzhko, R. R. Levitskii, and S. I. Sorokov, *Ukr. J. Phys.* **35**, 1421 (1990) (in Ukrainian).
- ³⁴J. Florencio, Jr. and M. H. Lee, *Phys. Rev. B* **35**, 1835 (1987).
- ³⁵U. Brandt and J. Stolze, *Z. Phys. B: Condens. Matter* **64**, 327 (1986); J. M. R. Roldan, B. M. McCoy, and J. H. H. Perk, *Physica A* **136**, 255 (1986); J. Stolze, V. S. Viswanath, and G. Müller, *Z. Phys. B: Condens. Matter* **89**, 45 (1992); M. Böhm, H. Leschke, M. Henneke, V. S. Viswanath, J. Stolze, and G. Müller, *Phys. Rev. B* **49**, 417 (1994); M. Böhm, V. S. Viswanath, J. Stolze, and G. Müller, *ibid.* **49**, 15669 (1994).
- ³⁶U. Brandt and K. Jacoby, *Z. Phys. B* **25**, 181 (1976); H. W. Capel and J. H. H. Perk, *Physica A* **87**, 211 (1977).
- ³⁷J. H. H. Perk and H. W. Capel, *Physica A* **92**, 163 (1978).
- ³⁸H. B. Cruz and L. L. Gonçalves, *J. Phys. C* **14**, 2785 (1981).
- ³⁹H. Bateman and A. Erdélyi, *Higher Transcendental Functions* (McGraw-Hill, New York, 1953), Vol. 2.
- ⁴⁰O. Derzhko and T. Krokhmalkii, *Phys. Rev. B* **56**, 11659 (1997); *Phys. Status Solidi B* **208**, 221 (1998).
- ⁴¹The modification of critical exponents due to competition of nearest-neighbor and next-nearest-neighbor interactions has also been observed recently in C. Trippé and A. Klümper, *Fiz. Nizk. Temp.* **33**, 1213 (2007); *Low Temp. Phys.* **33**, 920 (2007).
- ⁴²M. Kenzelmann, R. Coldea, A. A. Tennant, D. Visser, M. Hofmann, P. Smeibidl, and Z. Tylczynski, *Phys. Rev. B* **65**, 144432 (2002).
- ⁴³The results for $\Omega < 0$ can be obtained by symmetry after replacing Ω , K with $-\Omega$, $-K$.
- ⁴⁴H. Bateman and A. Erdélyi, *Higher Transcendental Functions* (McGraw-Hill, New York, 1953), Vol. 1.
- ⁴⁵M. V. Fedoryuk, *Mjetod Pjerjevala* (Nauka, Moskva, 1977) (in Russian).